The International Journal of Advanced Manufacturing Technology (2020) 107:3011–3022
https://doi.org/10.1007/s00170-020-05213-0

ORIGINAL ARTICLE

Prediction of the residual state of stress in a superduplex stainless steel produced by sand casting (using a coupled thermo-mechanical approach)

G. Palumbo[1] · A. Piccininni[1] · P. Guglielmi[1]

Received: 13 November 2019 / Accepted: 13 March 2020 / Published online: 1 April 2020

Abstract
The present work aims at investigating the effect, in terms of residual stress prediction, determined by the adoption of different material constitutive models in the Finite Element simulation of the casting process of a superduplex stainless steel benchmark, from the cooling after the pouring phase to the subsequent heat treatment (heating and water quenching). A 3D thermo-mechanical Finite Element (FE) model was created with the commercial code Abaqus: the preliminary thermal problem, i.e. the determination of the heat transfer coefficients during both the mould cooling and the quenching, was solved by means of an inverse analysis approach by minimizing the difference between the numerical evolution of temperature and the experimental acquisition coming from real casting test. Two separate routes were followed according to the adopted constitutive equations: modelling the material as (i) elasto-plastic or (ii) elasto-viscoplastic. The numerical prediction of the residual state of stress in terms of casting relaxation was compared with the experimental data after the cut of the casting using an electro-discharge machine. The analysis revealed that when the elasto-viscoplastic modelling was adopted, the simulations underestimated the relaxation with an error larger than 50%; on the other hand, the elasto-plastic model leads to an overestimation with an error of about 30%.

Keywords ASTM A890 Gr. 5A · Finite element method · Inverse analysis · Quenching · Residual stresses

1 Introduction

The performance of engineering components manufactured by means of foundry processes can be considerably influenced by several defects, among which one of the most detrimental is represented by the residual state of stress. If adjacent regions experience different specific volume variations (due to cooling at different rates or to different phase transformations), stresses can arise and if the yield limit of the material is overcome, a residual stress state remains at room temperature [1]. Such a defect is common in several industrial processes, like for example welding, partial (surface) or global heat treatments, and machining [2–4]. Components obtained by casting (especially sand casting) are generally subjected to heat treatments before further machining or being put in exercise: residual stresses generated during the cooling in the sand mould can have an influence on the final residual state at the end of the subsequent heat treatment. In particular, this aspect becomes crucial when dealing with the casting of large-scale components made of superduplex stainless steels (SDSS), mainly adopted for oil and gas applications, thanks to their high corrosion resistance due to the balanced biphasic austenitic-ferritic microstructure at room temperature [5]. During the cooling phase in the sand mould, beside the development of a stress state due to the differential cooling of adjacent regions of the cast, some embrittling secondary phase precipitation can be promoted, having a negative

✉ A. Piccininni
antonio.piccininni@poliba.it

G. Palumbo
gianfranco.palumbo@poliba.it

P. Guglielmi
pasquale.guglielmi@poliba.it

[1] Department of Mechanical Engineering, Mathematics & Management Engineering (DMMM), Politecnico di Bari, Bari, Italy

effect on toughness, ductility and corrosion resistance [6–8]. For this reason, a properly designed heat treatment after cooling in the sand mould becomes an unavoidable step to ensure the quality of the casting: at first, a preliminary heating up to a certain temperature (usually higher than 1100 °C) is necessary to enter the biphasic region of the phase diagram (where only ferrite and austenite coexist), subsequently followed by a drastic decreasing of temperature to freeze up the microstructure and avoid the risk of secondary phase precipitation [5]. Starting from this scenario, it should be clear that predicting the occurrence of such defects and, more than that, also the interactions between stress states generated by different processes on the component is a challenging problem. The FE approach represents a helpful and efficient tool in this direction: if the component is characterized by high level of complexity, such an approach can be used to minimize the costs related to the trial and error approach, thus assuring high quality and cheaper parts.

Numerical prediction of the residual state of stress needs the solution of both the thermal and the mechanical problem: a fully coupled approach within a FE environment [9] or, alternatively, the solution of the thermal problem with a finite difference (FD) solver and the subsequent mechanical one within a FE environment [10] are both reported in literature as viable solutions. The robustness of a numerical model can be ensured properly defining two key aspects: (i) the material modelling and (ii) the thermal boundary conditions. As for the former, several studies underline the importance of taking into account the viscous behaviour of the alloy during the cooling down [11–13]; otherwise, an overestimation of the residual state of stress at room temperature may result from a less complex elasto-plastic rheological model. On the other hand, the reduction of computational costs, without undermining the accurateness of the numerical prediction, is another key point: neglecting the presence of the sand mould, thus proposing an improved surface element formulation [14] able to take into account the effect of the mould constraint, or assuming that the heat transfer is mainly regulated by the convection laws [13] are reported to be promising solutions to shorten simulation time. As previously introduced, the thermal boundary conditions, i.e. the heat transfer coefficients (HTC), need to be properly determined. Despite several experimental methods can be considered effective (the immersion method, unidirectional tests, the one-dimensional solidification process, fluidity tests) [15], the adoption of the inverse analysis approach is still considered one of the most reliable solutions. Temperature-time curves are acquired by probes and used as target data to inversely determine the optimal value of the HTC by means of the minimization of an error function [13, 16]. In particular, the inverse analysis gives more advantages especially when applied to the solution of complex thermal problems, as in the case of water quenching processes: differently from the case of gas (or air) quenching numerical simulations, in which the computational fluid dynamics (CFD) provides a reliable estimation of the HTCs as function of temperature [17, 18], the water quenching process is characterized by an even more complex interaction between the component and the quenchant [19] and, at the same time, it is influenced by a larger number of parameters, as the entering position of the component in the quenching bath or the flow rate and agitation of the quenchant [20, 21]. The adoption of the inverse analysis to evaluate the HTCs is widely reported to be effective, especially if coupled with various optimization procedures [16, 22–24].

The present work deals with the investigation on the evolution of the residual stress state in a cast benchmark superduplex stainless steel (ASTM A890 Gr. 5A) component during the whole manufacturing process. After cooling down in the mould, the cast component was subjected to a subsequent heat treatment: at first, it was heated up to 1130 °C (in the region of the austenitic-ferritic biphasic region) to relief the arisen residual state of stress and to eliminate any secondary phases in the microstructure. The part was then water quenched to freeze up the characteristic biphasic structure of SDSS as also proved by subsequent metallographic investigations. On the other hand, the whole manufacturing process was numerically investigated adopting a fully coupled thermo-mechanical approach. According to Palumbo et al. [13], the HTC (as a function of temperature) were inversely determined minimizing the difference between the numerical and the experimental time evolution of temperature in specific points of the casting. To evaluate the effect of the material modelling on the stress prediction, two separate routes were investigated: (i) an elasto-plastic constitutive modelling implementing temperature-dependent flow stress curve or (ii) an elasto-viscoplastic constitutive equation adding the viscous contribution implementing data from the creep tests.

2 Material and methods

2.1 Investigated material and geometry of the case study

In this section, a brief description of the investigated material and the adopted geometry is provided, being these aspects already discussed in the previous work of the same authors

Table 1 ASTM A890 Gr5A chemical composition (wt%)

C %	Cr %	Ni %	Mo %	N %
< 0.03	25.0	7	4.2	0.18

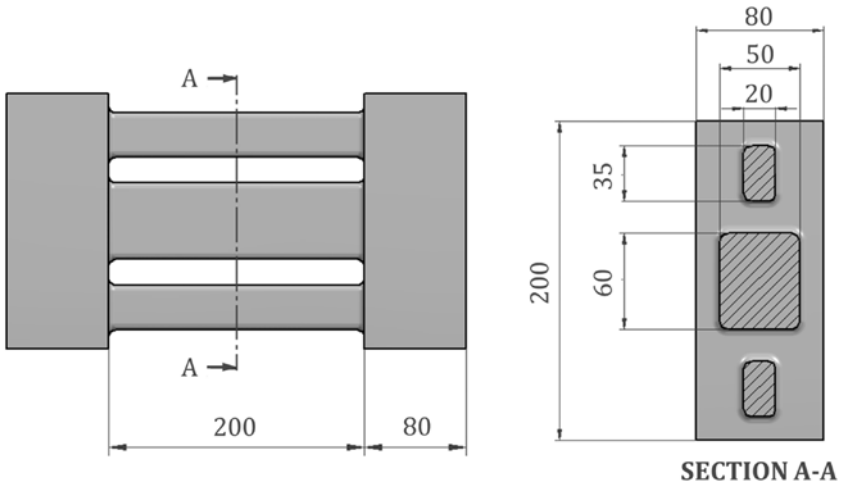

Fig. 1 Overview of the investigated geometry with the main quotes in millimeters

[13]: the investigated alloy, namely ASTM A890 Gr. 5A, belongs to the group of the superduplex stainless steels, considered particularly interesting since it is characterised high mechanical properties and higher corrosion resistance than the conventional austenitic grades [5]. The chemical composition of the alloy is resumed in Table 1.

The investigated benchmark geometry, widely adopted in literature [13, 25], is a casting consisting of three bars characterized by unbalanced moduli able to promote the occurrence of a residual state of stress. The main dimensions of the investigated geometry are reported in Fig. 1.

2.2 Water quenching

In the present work, the residual state of stress was numerically predicted at the end of the water quenching step. Figure 2 schematically reports the complete thermal history experienced by the node located on the middle plane of the side bar (highlighted in green): once reaching the room temperature after the first two steps (BSO "before shake out" and ASO "after shake out"), the component was fully solutioned by means of a specific heat treatment (HT) and subsequently water quenched (WQ).

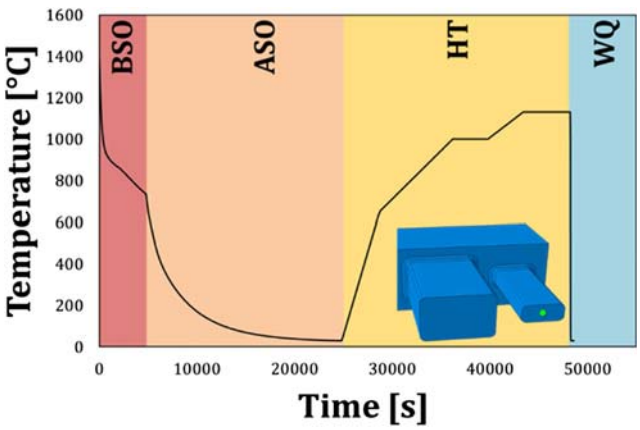

Fig. 2 Description of the thermal history during the whole process experienced by the node located on the middle plane of the side bar

During the HT and WQ phases, the casting temperature was monitored by means of K-type thermocouples (acquisition frequency equal to 1 Hz) located both on the outer surface of the bars and near the casting middle plane (respectively indicated as Surface TC and Middle Plane TC in the 3D schematic representation of Fig. 3a).

Once cooled down at room temperature, the casting was heat-treated following the temperature profile showed in Fig. 3b. The heat treatment was carried out in an industrial furnace (Fig. 4a) and, after the cast reached a homogeneous temperature of 1130 °C, it was immersed in a quenching bath (Fig. 4b) that was continuously fed by a constant water flow rate to maintain its temperature as close as possible to the room one.

2.3 The stress relaxation technique

The residual state of stress after quenching was evaluated adopting the stress relaxation technique [26], being such a procedure considered one of the destructive techniques often adopted to estimate of the residual state of stress in the as-cast condition, i.e. once the cooling phase (after the pouring) was finished. Both the side bars were subjected to consecutive cuts (according to the sequence in Fig. 5) by means of a 0.3 mm wire electro discharge machine (EDM).

A physical reference point (Ref) for the initial wire positioning was created on one of the massive parts of the casting; the wire was then moved in the position of the first cut and its coordinates were recorded. After the first cut (1A in Fig. 5), the two halves came in contact, completely enclosing the gap created by the wire, due to a partial relaxation of the residual stress state. The complete

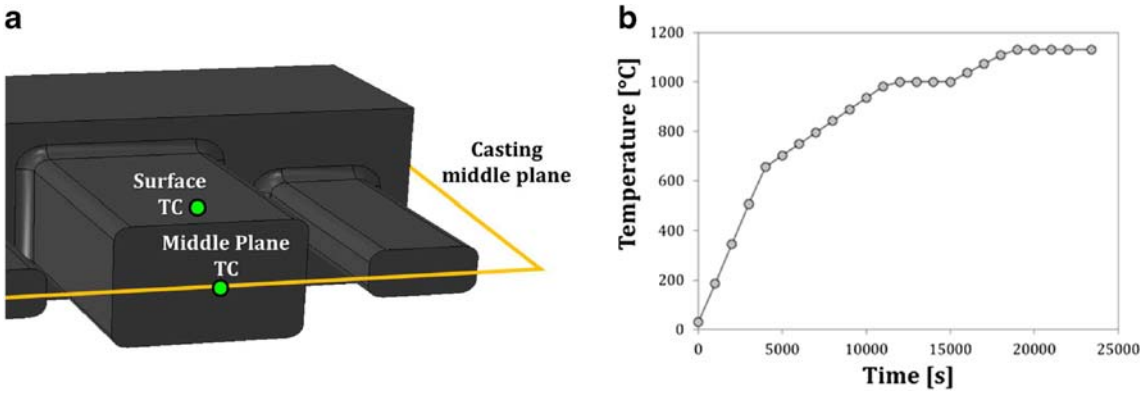

Fig. 3 K-type thermocouples positioning (**a**) and temperature evolution during the heating phase (**b**)

relaxation on the first bar was ensured after the second cut (2A in Fig. 5) located 5 mm far from the first one along the longitudinal direction. The same procedure was applied on the other side bar, sequentially cutting along 1B and 2B, so that the state of stress in both the bars could be completely relaxed. The wire was then positioned in contact with the first bar at the 1A cut location: the current coordinates were again recorded and compared with those acquired before the 1A cut to experimentally evaluate the bar relaxation.

2.4 Metallographic investigations

Metallographic analyses were performed by means of light microscopy and exploiting the Struers® LectroPol5. The two slices (5 mm thick) from the consecutive cuts on the side bar cutting were further investigated via metallographic analyses using an electrolytic polishing (using the Struers® A3 electrolyte) and a subsequent electrochemical etching (in a 20% NaOH aqueous solution at 3.5 V for 5 s).

Results at different magnifications in Fig. 6 a and b show that, at the end of the quenching process, the microstructure was characterized by the presence of isles of austenite (appearing brighter) in a ferritic matrix; the black dots are relative to microporosities due to the casting process, while no sigma phase was found (such a brittle phase can be easily distinguished from the austenite and ferrite, appearing orange or dark brown in a micrograph, depending on the adopted magnification [27]).

2.5 Description of the numerical procedure

The fully coupled thermo-mechanical approach was adopted; only half of the casting was modelled to sensibly reduce the computational costs: the geometry was meshed with 12346 C3D8T (8-node thermally coupled brick, trilinear displacement and temperature available in the Abaqus element library) elements with an average size of 5 mm. The whole casting process was simulated: from the initial cooling phase (BSO and ASO in Fig. 2) to the heat treatment that was divided into two sub-steps; in the first step, i.e. the heating phase, the simulation time was set to 23,400 s (this is the real duration of the heating in the furnace), whereas in the second one, i.e. the water quenching, the simulation time was set to 400 s, which is the time the bars needed to cool down to the room temperature. The accuracy of the proposed numerical

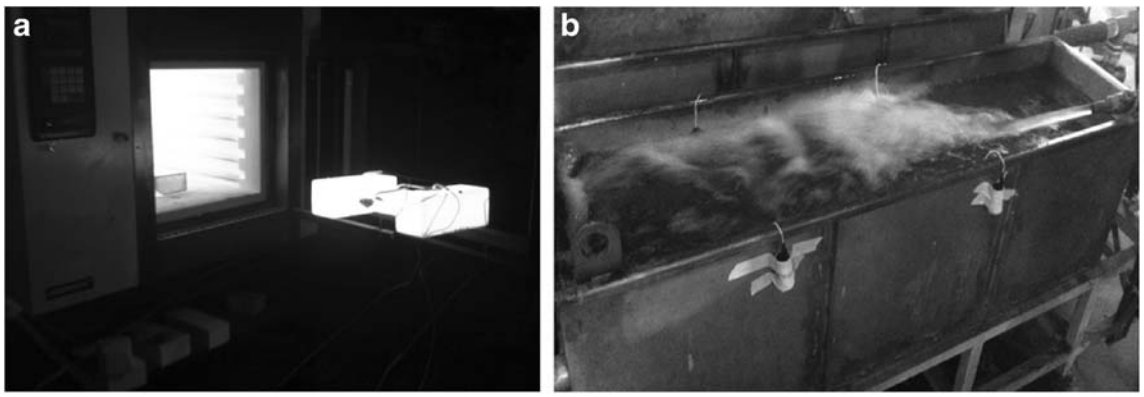

Fig. 4 Industrial furnace for heating up the casting (**a**). Water bath adopted for the quenching (**b**)

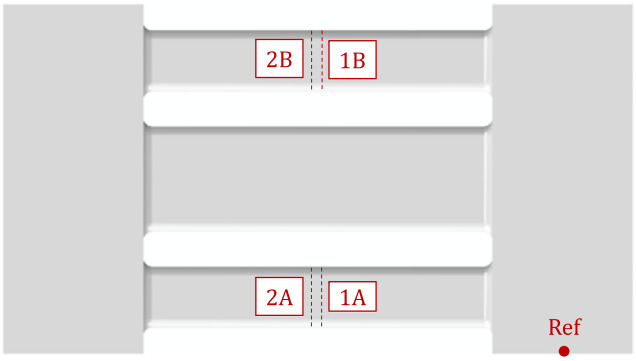

Fig. 5 Sequence of cuts by means of EDM wire cut

model relies on two key points: (i) the material behaviour and (ii) the definition of the thermal boundary conditions. As for the former aspect, the influence of the constitutive equation was evaluated throughout the whole process, from the initial cooling step up to the final water quenching. The material data have been briefly recalled from a previous work [13]: uniaxial tensile tests suggested that the material yield point decreased as the temperature increased (curve labelled as σ_y in Fig. 7a); additional uniaxial tensile tests were carried to specifically determine the elastic behaviour of the material [28] showing a similar dependence of the Young's modulus according to the temperature (curve labelled as E in Fig. 7a).

Material data were arranged to be subsequently implemented within the FE model: in particular, results from the tensile tests were fitted by means of the Hollomon's model ($\sigma = K\varepsilon^n$) whose constants are plotted in Fig. 7b as a function of the test temperature (the material behaviour was modelled as perfectly plastic at temperature higher than 800 °C).

On the other hand, the material viscous behaviour was investigated by means of creep tests at high temperatures, namely 600 °C, 800 °C and 1000 °C: tests were carried out up to the secondary stage and results were fitted using the Norton-Bailey power law ($\dot{\varepsilon} = A\sigma^b$), whose constants have been listed in Table 2 according to the temperature levels.

The above presented results were subsequently implemented within the FE model allowing to investigate two different formulations: (i) an elasto-viscoplastic (EVP) constitutive model and (ii) an elasto-plastic (EP) constitutive equation.

As concerning the thermal boundary conditions, HTCs were properly evaluated by means of the inverse analysis applied on pure thermal transient simulations: the casting geometry was partitioned as shown in Fig. 8a and, for each portion, HTCs as a function of the temperature (both in the cooling phase after pouring [13] and in the water quenching) were determined minimizing the error between the numerical evolution of temperatures and the experimental data coming from the thermocouples (as described in Section 2.2).

Material thermal properties—i.e. thermal conductivity, density and specific heat—were modelled as a function of temperature implementing data from a previous experimental campaign [16]. The stress state at the end of quenching (calculated by means of a fully coupled thermo-mechanical analysis) was imported in the subsequent mechanical simulation and the bar relaxation was numerically evaluated removing the symmetry constraints on the side bars (highlighted in orange in Fig. 8a).

As depicted in Fig. 8b, the relaxation was determined as the absolute value of the difference between the component along the y axis of the segment AB (end of the quenching) and the segment AB' (once the stress state was relaxed).

3 Results

3.1 HTC numerical evaluation

The HTCs, which regulate the heat exchange between the casting and the quenchant (water, in this case), play a key role in the simulation and need to be correctly evaluated.

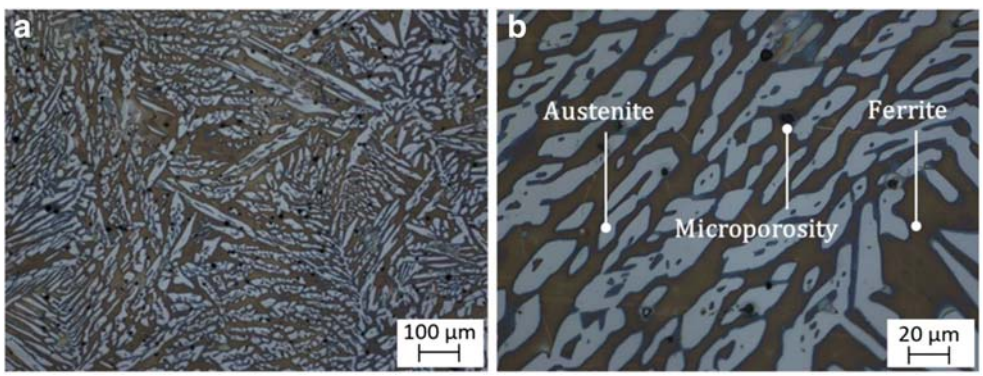

Fig. 6 Results of the metallographic investigation: 10× (**a**) and 50× (**b**)

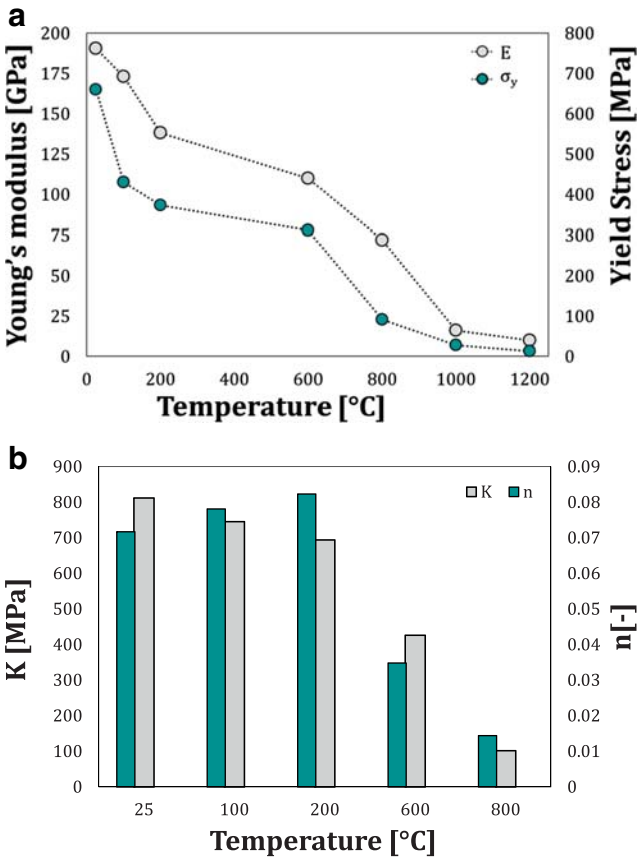

Fig. 7 Results from the uniaxial tensile tests. **a** Yield point and **b** Young's modulus as a function of the test temperature

Temperature evolutions during the water quenching were acquired by thermocouples placed at the middle plane of the casting (Middle Place TC in Fig. 3a) and used as target data for a robust evaluation of the HTCs.

As the bold lines in Fig. 9 show, high cooling rates were achieved during the quenching: only few seconds were necessary to decrease the temperature from the one at the end of the heating (1130 °C) down to the room one.

The good matching between the numerical results (dashed lines with markers) and the experimental data (continuous lines) on both bars confirms the effectiveness of the adopted approach based on the inverse analysis. The resulting HTC profiles for each of the partitioned region have been reported in Fig. 10 a and b according to temperature.

Table 2 Creep tests at high temperature: material constants of the Norton-Bailey power law

Temperature (°C)	A ($MPa^{-b}·s^{-1}$)	*b* (−)
600	4.65E−23	6.9587
800	7.85E−13	4.2429
1000	2.36E−09	3.5198

3.2 Numerical evolution of the residual state of stress

The evolution of the residual stress state was numerically investigated throughout the whole casting process, considering both the EP and the EVP constitutive model.

When neglecting the viscous contribution (Fig. 11 a and b), during the first cooling after pouring, both of the bars were subjected to an uniaxial state of stress, tensile for the middle bar and compressive for the side bars.

During the subsequent heating, the state of stress was not completely relieved in both bars as shown in Fig. 11 c and d. Due to the high cooling rate of the water quenching, the casting experienced a much higher (in module) stress state, more complex and not completely uniaxial: the minimum principal stress component in the middle bar (Fig. 11e) was lower than the maximum principal one, but not so much to be considered negligible (about 200 MPa), whereas the side bar was stressed in the opposite way (Fig. 11f).

Similar trends were identified monitoring the evolution of the residual stress in the casting when adopting the EVP constitutive model (Fig. 12a–f): the most evident difference was that, at the end of the heating step, residual stresses were almost completely absent; in addition, the stress level after the quenching step resulted again to be more complex, but lower than the one implementing the EP constitutive model. It is important to point out that, regardless of the adopted material constitutive equation, the stress state at the end of the quenching step was much more complex than the one in the as-cast condition (i.e. after solidification in the mould).

3.3 Numerical evaluation of the bar relaxation

EDM wire cuts were modelled removing the symmetry constraints on the side bars: since bar relaxation is directly connected with the final stress state at the end of the quenching, the Mises stress distribution of the side bar along the vertical path shown in Fig. 13 was investigated.

The stress distribution in the as-cast condition resulted to be almost constant along the cross section both in the case of the EP (a) and the EVP (b) constitutive model; on the contrary, only in the case of the elasto-plastic behaviour, a less uniform stress distribution was obtained at the end of the quenching step.

The bar relaxation was numerically calculated as explained in Section 2.5 (Fig. 8b) and results have been reported in Table 3: it is evident that, when implementing the EVP constitutive model, the numerical prediction of the bar relaxation

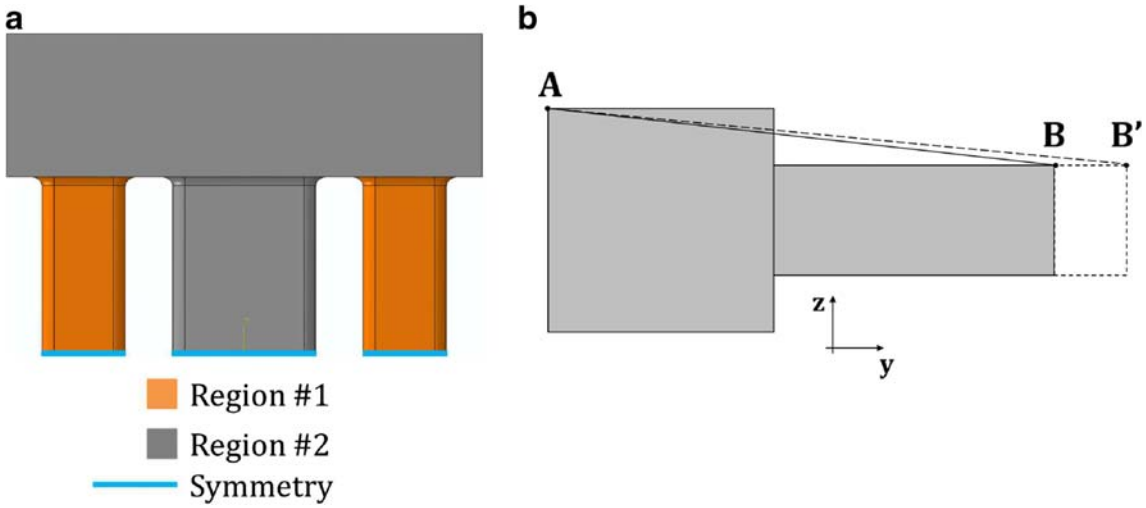

Fig. 8 Casting division for the HTC evaluation (**a**). Scheme for the numerical determination of the bar relaxation (**b**)

resulted sensibly lower than in the case the viscous contribution was neglected.

4 Discussion of results

The inverse analysis through the minimization of an error function resulted to be effective in providing proper thermal boundary conditions: the resulting HTC curves as a function of temperature proposed in Fig. 10 a and b are in good accordance with the theory: the peak value is in the region of the lower temperatures and its value is comparable with data available in literature for the P20 steel [24], an eutectoid steel [29] and the SUS304 stainless steel [22].

As reported in Section 3.2, the choice of the constitutive equation strongly affected the residual state of stress at the end of the cooling in the mould: during the heating step, the stress state of both bars (Fig. 14 a and b) predicted by the FE simulation implementing the EVP model was characterized by a pronounced drop after around 3200 s.

In addition, at the end of this heating step, a residual uniaxial compressive state (around 10 MPa) was found on the side bar when neglecting the viscous behaviour (Fig. 15a); on the contrary, at the end of the heating,

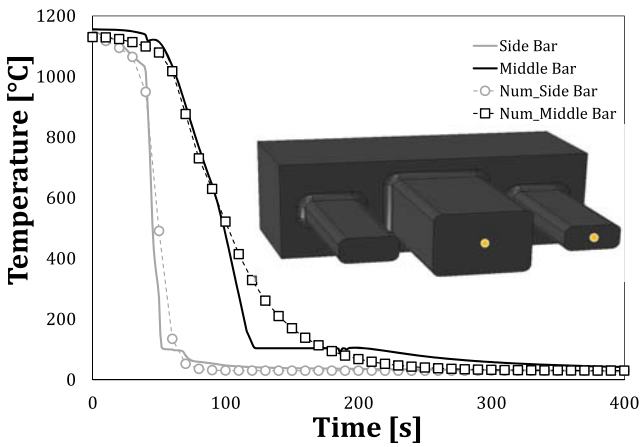

Fig. 9 Numerical vs. experimental evolution of temperature during quenching

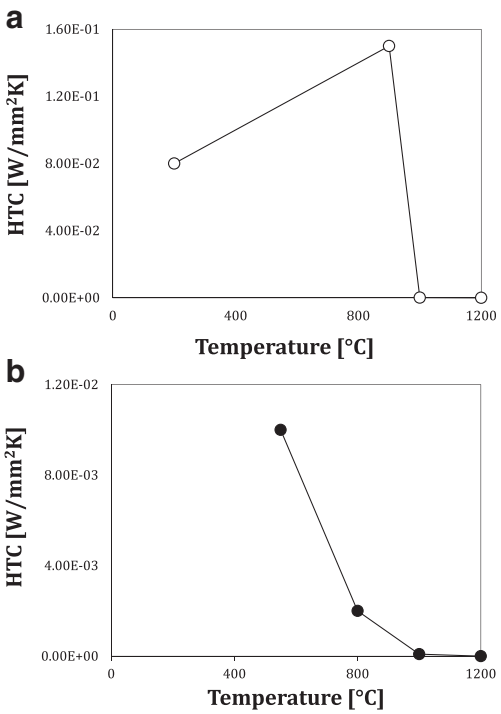

Fig. 10 HTC profiles. Region#1 (**a**). Region#2 (**b**)

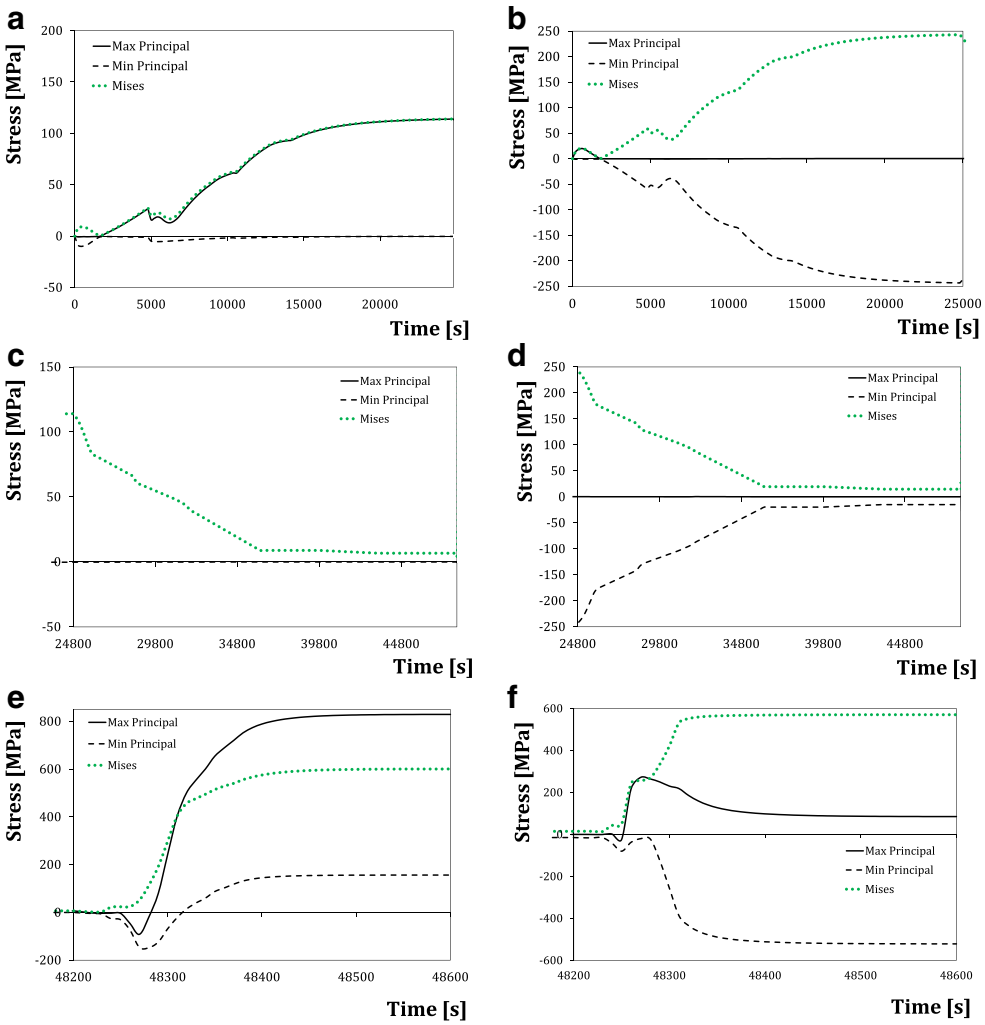

Fig. 11 EP material modelling, evolution of residual stress. Middle bar (**a**) and side bar during cooling after pouring (**b**). Middle bar (**c**) and side bar during heating (**d**). Middle bar (**e**) and side bar during water quenching (**f**)

almost the entire residual stress was relieved in the case of the simulation implementing the EVP material model (Fig. 15b).

Material modelling resulted to have a not negligible influence on the final stress state at the end of the quenching step: the contribution of the viscous behaviour is evident in the final maximum principal stress of the middle bar, remarkably lower than the one predicted when such a contribution was neglected (Fig. 16a).

A similar trend was found in the side bar, characterized by a final value of the minimum principal stress much higher (more than twice) than in the case the EP material model was adopted (Fig. 16b). If compared with the almost completely uniaxial state of stress in the as-cast conditions—i.e. after the steps BSO and ASO—the more complex and severe state of stress justified the higher relaxation of the side bars.

It can be thus stated that once the boundary thermal conditions are properly defined, the accurateness of the numerical prediction depends only on the choice of the proper constitutive equation. As shown in Fig. 17, neglecting the viscous contribution in the material behaviour led to an overestimation of the as-cast residual stress state at room temperature, twofold higher than the one calculated implementing the EVP material model.

On the contrary, the EP model, despite overestimating the experimental data of about 30%, resulted to be more accurate than the EVP formulation, according to which the bar relaxation was underestimated of more than 50%.

The extensive knowledge of both the plastic and viscous properties was confirmed to be of prior importance to adequately model the material behaviour in the FE model, but the choice of the proper constitutive equation was important as well, in order to avoid poor accuracy in the estimation of the residual state of stress.

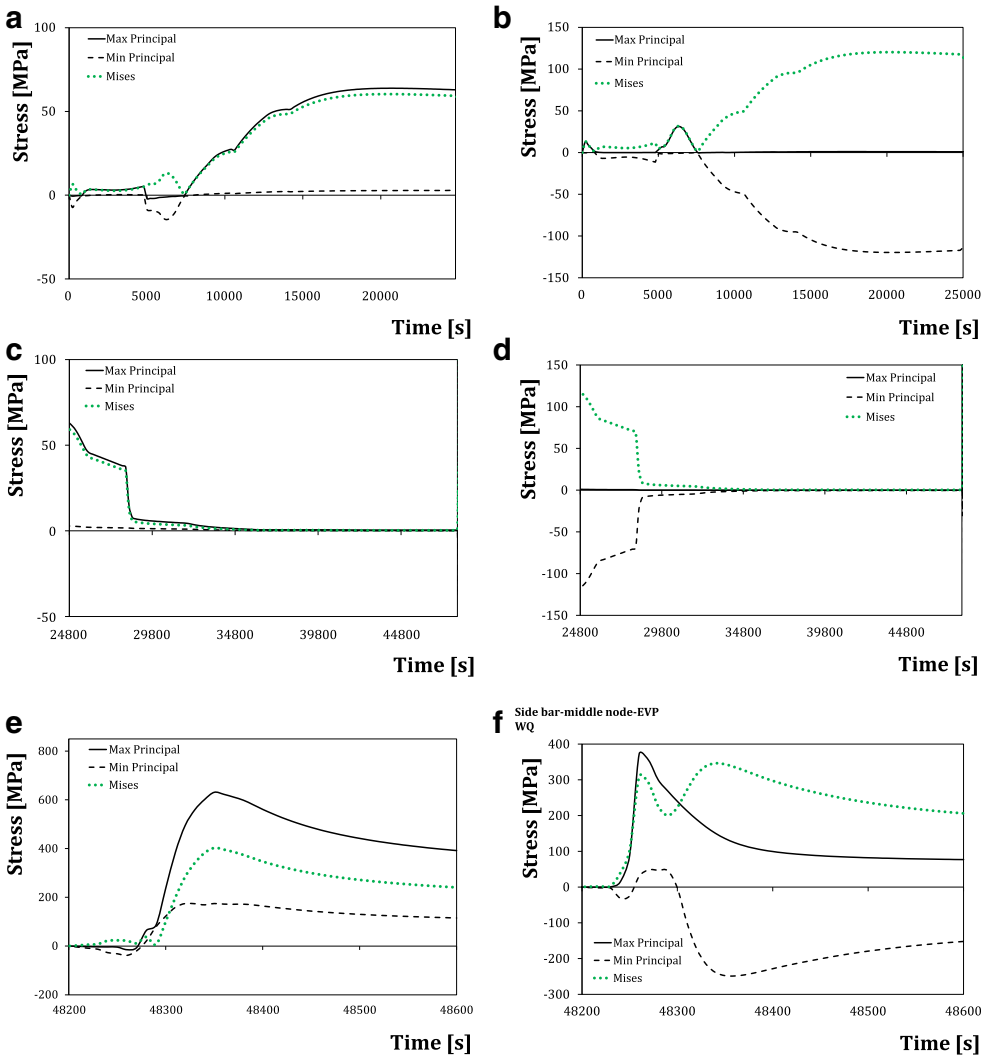

Fig. 12 EVP material modelling, evolution of residual stress. Middle bar (**a**) and side bar during cooling after pouring (**b**). Middle bar (**c**) and side bar during heating (**d**). Middle bar (**e**) and side bar during water quenching (**f**)

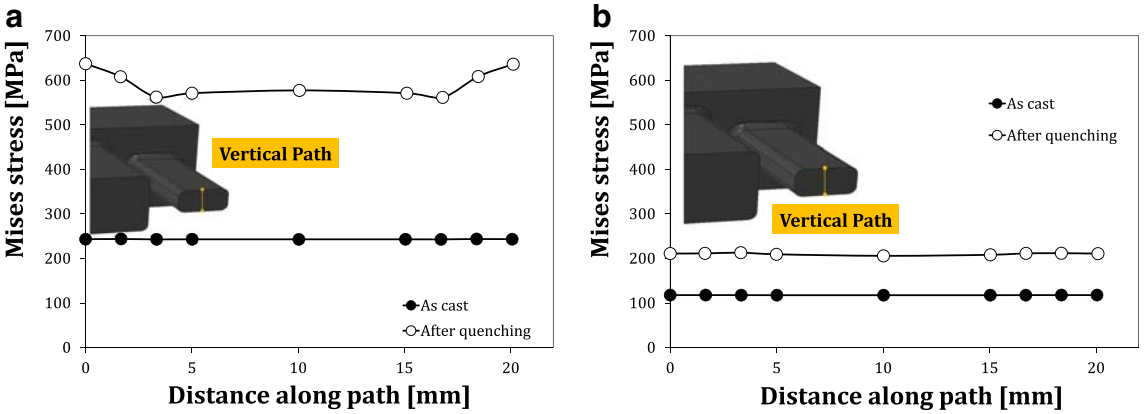

Fig. 13 Comparison of the equivalent stress on the side bar in the as-cast condition and after quenching. EP (**a**). EVP (**b**)

Table 3 Numerical estimation of the side bar displacement due to stress relaxation

	As cast [13]	After quenching
Numerical (EVP)	0.069 mm	0.12 mm
Numerical (EP)	0.143 mm	0.35 mm

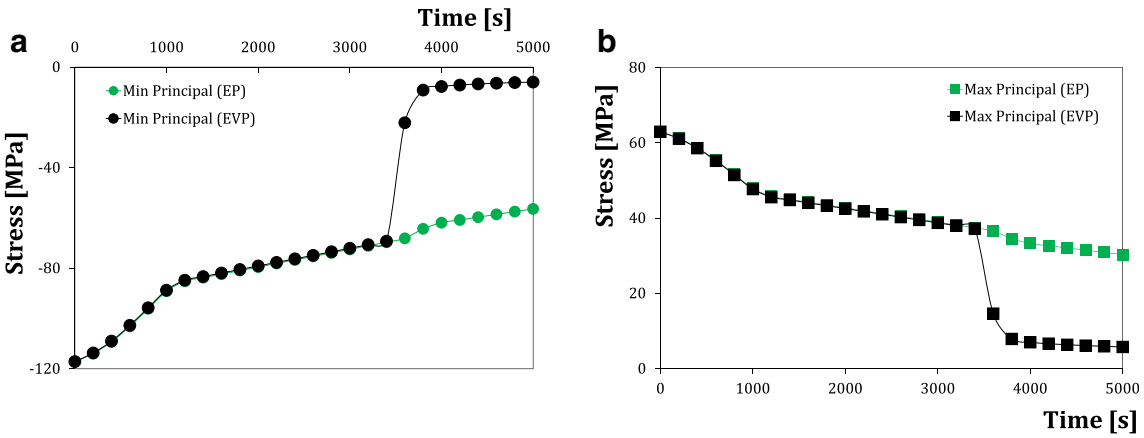

Fig. 14 Creep contribution on the stress evolution during the heating phase. Side bar (**a**) and middle bar (**b**)

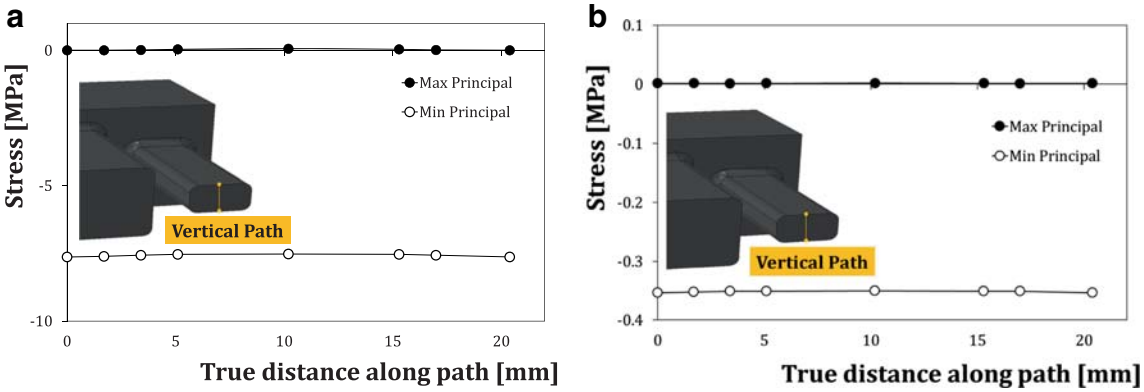

Fig. 15 Residual stresses in the cross section of the side bar at the end of the heating phase. EP (**a**). EVP (**b**)

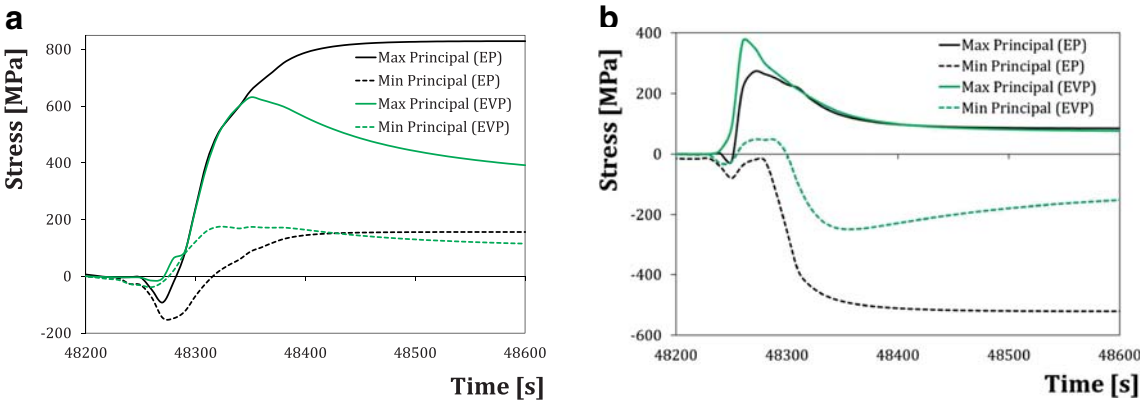

Fig. 16 Influence of the material modelling on the final stress state after quenching. The middle bar (**a**) and the side bar (**b**)

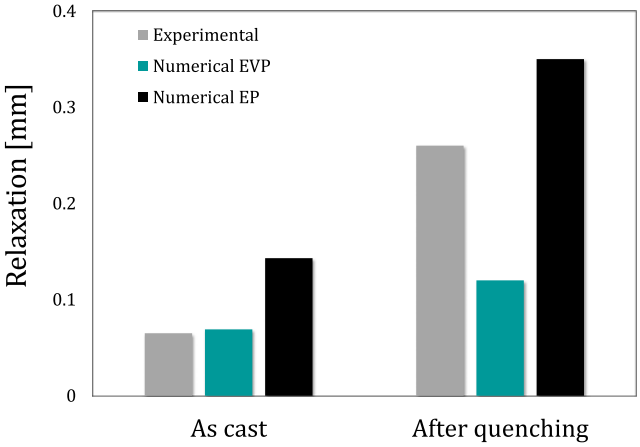

Fig. 17 Numerical vs. experimental side bar relaxation in the as-cast and after quenching conditions

5 Conclusions

The prediction of the residual state of stress during the whole casting process, from the mould cooling to the final water quenching, has been successfully assessed in the present work, thanks to (i) the proper definition of the thermal boundary conditions and (ii) the in-depth investigation of the influence of the material constitutive behaviour. The attention has been focused to a benchmark widely adopted in literature [13, 25], consisting of three bars characterized by unbalanced moduli able to promote the occurrence of a residual state of stress.

The inverse analysis revealed to be a robust methodology able to accurately evaluate the HTCs starting from experimental data: the thermal history of the casting was simulated with an optimal fitting between experimental and numerical data.

Such an approach allowed to focus the attention in this work on the material constitutive modelling, which revealed to play a key role in the prediction of the residual stress state, especially in the case of a more complex stress state like the one occurring after the water quenching.

Although the EVP formulation proved its effectiveness in precisely predicting the residual state of stress in the as-cast condition (overestimating experimental measurements of less than 7% [13]), the EP material modelling gave a more accurate prediction of the residual state of stress after the quenching (overestimating the experimental measurement of about 30%).

The proposed results represent an additional step towards the improvement of the reliability of a FE-based design tool able to predict even very complex stress states as the ones at the end of a quenching step: as revealed by the investigations conducted by the authors, not only the heat transfer but also the material modelling has to be properly tuned in order to avoid poor accuracy of the results.

Acknowledgments The present work arose from activities conducted in the project SMATI, funded in the framework of the European National Operative Programme for Research and Competitiveness and coordinated by Prof. Luigi Tricarico, to whom the authors are grateful for the support and the guidance.

References

1. Totten G, Howes M, Inoue T (2002) Handbook of residual stresses and deformation of steel, ASM International
2. Vasantharaja P, Vasudevan M, Palanichamy P (2014) Effect of welding processes on the residual stress and distortion in type 316LN stainless steel weld joints. J Manuf Process. https://doi.org/10.1016/j.jmapro.2014.09.004
3. Kong F, Ma J, Kovacevic R (2011) Numerical and experimental study of thermally induced residual stress in the hybrid laser–GMA welding process. J Mater Process Technol 211:1102–1111. https://doi.org/10.1016/j.jmatprotec.2011.01.012
4. García Navas V, Gonzalo O, Bengoetxea I (2012) Effect of cutting parameters in the surface residual stresses generated by turning in AISI 4340 steel. Int J Mach Tools Manuf 61:48–57. https://doi.org/10.1016/j.ijmachtools.2012.05.008
5. Mc Guire MF (2008) Stainless steel for design engineers, ASM International
6. Wang YQ, Han J, Wu HC, Yang B, Wang XT (2013) Effect of sigma phase precipitation on the mechanical and wear properties of Z3CN20.09M cast duplex stainless steel. Nucl Eng Des 259:1–7. https://doi.org/10.1016/j.nucengdes.2013.02.037
7. Chan K, Tjong S (2014) Effect of secondary phase precipitation on the corrosion behavior of duplex stainless steels. Materials (Basel) 7:5268–5304. https://doi.org/10.3390/ma7075268
8. Fargas G, Mestra A, Mateo A (2013) Effect of sigma phase on the wear behavior of a super duplex stainless steel. Wear 303:584–590. https://doi.org/10.1016/j.wear.2013.04.010
9. Si H-M, Cho C, Kwahk S-Y (2003) A hybrid method for casting process simulation by combining FDM and FEM with an efficient data conversion algorithm. J Mater Process Technol 133:311–321. https://doi.org/10.1016/S0924-0136(02)01008-7
10. Fackeldey M, Ludwig A, Sahm PR (1996) Coupled modelling of the solidification process predicting temperatures, stresses and microstructures. Comput Mater Sci 7:194–199. https://doi.org/10.1016/S0927-0256(96)00080-8
11. Fachinotti VD, Cardona A (2003) Constitutive models of steel under continuous casting conditions. J Mater Process Technol 135:30–43. https://doi.org/10.1016/S0924-0136(02)00955-X
12. Koric S, Thomas BG (2008) Thermo-mechanical models of steel solidification based on two elastic visco-plastic constitutive laws. J Mater Process Technol 197:408–418. https://doi.org/10.1016/j.jmatprotec.2007.06.060
13. Palumbo G, Piccininni A, Piglionico V, Guglielmi P, Sorgente D, Tricarico L (2015) Modelling residual stresses in sand-cast superduplex stainless steel. J Mater Process Technol 217:253–261. https://doi.org/10.1016/j.jmatprotec.2014.11.006
14. Metzger D, Jarrett New K, Dantzig J (2001) A sand surface element for efficient modeling of residual stress in castings. Appl Math Model 25:825–842. https://doi.org/10.1016/S0307-904X(01)00017-8
15. Nishida Y, Droste W, Engler S (1986) The air-gap formation process at the casting-mold interface and the heat transfer mechanism through the gap. Metall Trans B 17:833–844. https://doi.org/10.1007/BF02657147
16. Palumbo G, Piglionico V, Piccininni A, Guglielmi P, Sorgente D, Tricarico L (2015) Determination of interfacial heat transfer coefficients in a sand mould casting process using an optimised inverse

analysis. Appl Therm Eng 78:682–694. https://doi.org/10.1016/j.applthermaleng.2014.11.046
17. Elkatatny I, Morsi Y, Blicblau AS, Das S, Doyle ED (2003) Numerical analysis and experimental validation of high pressure gas quenching, 42:417–423. https://doi.org/10.1016/S1290-0729(02)00042-X
18. Xiao B, Wang Q, Wang G, Sisson RD, Rong Y (2010) Robust methodology for determination of heat transfer coefficient distribution in convection. Appl Therm Eng 30:2815–2821. https://doi.org/10.1016/j.applthermaleng.2010.08.017
19. Handbook of heat treating, ASM International, 1991
20. Sedighi M, McMahon CA (2000) The influence of quenchant agitation on the heat transfer coefficient and residual stress development in the quenching of steels. Proc Inst Mech Eng Part B J Eng Manuf 214:555–567. https://doi.org/10.1243/0954405001518251
21. Fernandes P, Prabhu KN (2007) Effect of section size and agitation on heat transfer during quenching of AISI 1040 steel, 183:1–5. https://doi.org/10.1016/j.jmatprotec.2006.08.028
22. Sugianto A, Narazaki M, Kogawara M, Shirayori A (2009) A comparative study on determination method of heat transfer coefficient using inverse heat transfer and iterative modification. J Mater Process Tech 209:4627–4632. https://doi.org/10.1016/j.jmatprotec.2008.10.016
23. Li MEI, Allison JE (2007) Determination of thermal boundary conditions for the casting and quenching process with the optimization tool. OptCast 38:567–574. https://doi.org/10.1007/s11663-007-9076-8
24. Huiping L, Guoqun Z, Shanting N, Yiguo L, Inverse heat conduction analysis of quenching process using finite-element and optimization method, m (2006) 1087–1096. https://doi.org/10.1016/j.finel.2006.04.002
25. Gustafsson E, Hofwing M, Strömberg N (2009) Residual stresses in a stress lattice—experiments and finite element simulations. J Mater Process Technol 209:4320–4328. https://doi.org/10.1016/j.jmatprotec.2008.11.025
26. Schajer GS (2011) Destructive methods for measuring residual stresses: techniques and opportunities. Conf Proc Soc Exp Mech Ser 6:221–231. https://doi.org/10.1007/s11340-010-9386-7
27. ASM Handbook Volume 9: Metallography and microstructures, Vander Voo, ASM International, 2004
28. ISO 6892-2, Metallic materials – Tensile testing – Part 2: Method of test at elevated temperature, 2011
29. Kang S, Im Y (2007) Three-dimensional thermo-elastic – plastic finite element modeling of quenching process of plain-carbon steel in couple with phase transformation, 49:423–439. https://doi.org/10.1016/j.ijmecsci.2006.09.014